Effect of illumination wavelength on optimizing multi-camera location systems in a factory environment

Stuart Robson[1], Lindsay MacDonald[1], Stephen Kyle[1], Mark Shortis[2]

[1] Dept of Civil, Environmental and Geomatic Engineering, UCL, London WC1E 6BT
s.robson@ucl.ac.uk, lindsay.macdonald@ucl.ac.uk, s.kyle@ucl.ac.uk

[2] School of Mathematical and Geospatial Sciences, RMIT University, Melbourne
mark.shortis@rmit.edu.au

Abstract *As a model for a full-scale, factory-wide system, a system for dimensional measurement has been constructed using eight low-cost monochrome cameras with C-mount lenses on a rigid metal framework. The cameras were synchronised to capture simultaneous image sets, and photogrammetric software used to locate in each image the centroids of retroreflective targets on a 3D test object. The distortion parameters of the lens on each camera were estimated, and a target network constructed to a precision of better than 4.5 μm (at k=1), equivalent to a 1:220,000 discrimination range. Targets were illuminated by an annular LED ring attached to the front mounting ring of the lens of each camera, and the analysis was repeated for four different LED wavelengths.*

1. Introduction

The Light Controlled Factory (LCF) project is developing new methods for multi-dimensional measurement and tracking of assembly machines and parts in shop floor production. Specific objectives of the research programme are:

(i) To investigate assembly alignment and machine position controlled in real time by Large Volume Metrology (LVM) systems to a positional accuracy of between 10 and 250 μm over assemblies in the range 10 to 30 metres;
(ii) To specify and develop innovative techniques for establishing and compensating for environmental uncertainty on the dimensional fidelity of large assembly tools and parts (5 to 30 metres) and their tolerance stack-up;
(iii) To design and implement a novel, ubiquitous 7D (6DOF and time) measurement environment for the entire factory space, to provide graduated positional accuracy from 10 to 500 μm.

Given the importance of this precise measurement capability for high-quality manufacturing, there is great interest in optimising the performance of a multi-

camera 7D photogrammetric system for real-time factory operation (Peggs *et al,* 2009*)*. The role of the research group at UCL in the project is to enhance the accuracy of optical LVM systems by quantifying and modelling optical effects caused by environmental variations. This challenge is being addressed by developing a network of low-cost photogrammetric sensors able to measure the position of many thousands of target locations. With multi-camera, real-time triangulation of targeted points using high-quality retro-reflective targets and detailed camera models we aim to minimise systematic pointing errors. To characterise the environmental sensitivity of the system, we are also investigating the use of LED sources to illuminate the targets at narrow wavebands in the visible and near infra-red spectrum.

The widespread availability of digital camera systems equipped with either RGB mosaic (Bayer) filters, or separate filtered sensors, able to deliver three-channel colour images has prompted several investigations into camera calibration. Studies have concentrated on modelling and correcting distortions in the three colour channels and then recombining the images (Mallon and Whelan, 2007) or working through an extended RGB photogrammetric camera model (Luhmann *et al*, 2006) to provide image coordinate corrections. The precision was invariably limited by the broad spectral imaging properties of the sensors with their three band outputs.

Low-cost monochrome cameras with CMOS sensors and C-mount lenses have been successfully applied to a wide variety of metrology tasks. For high accuracy measurement, such cameras are typically equipped with ring lights to image retro-reflective targets as high contrast image features. Research in a related project, LUMINAR, assessed the effect of wavelength on camera calibration parameters for a C-mount wide-angle lens (Robson *et al*, 2014). White light from a studio flash was filtered through a series of narrow-band transmission filters at intervals of 20nm throughout the spectrum. Results demonstrated the strong influence of illumination wavelength on principal distance, radial and tangential distortion, and also possible trends in the parameters for principal point, orthogonality and affinity.

The current study builds on the previous results, using an 8-camera configuration in a rigid framework mounted on an optical bench to simulate at small scale the factory measurement situation. All eight camera bodies are identical, but for comparative investigation six different C-mount lenses have been used, with focal lengths ranging from 3.8mm (fish-eye) to 10mm. Also the illumination of the targets is now achieved by an annular LED ring attached in front of each lens rather than by a filtered flash. In this paper we report the results of testing photogrammetric performance with four different LED illumination wavelengths: broadband white light and three narrowband sources of red, green and blue.

2. Photogrammetric Target Detection

Our approach is to use photogrammetry to determine the image point correspondence in a multiple image network. Photogrammetric bundle adjustment refines parameters for the perspective camera model, target image locations and selected target coordinate datum with high levels of precision and reliability (Luhmann, 2011). The network setup is implemented in a digital close-range photogrammetry system, called the Vision Metrology System (VMS), where the retro-reflective targets, which form the basis of the initial sparse triangulation, have been identified in image sets. The VMS software, developed over the past 20 years, has been used effectively in industrial applications where very accurate measurements are required with a discrimination range between 1:10000 and 1:100000 (Shortis *et al,* 2001). The software analyses multiple images captured from an object marked with targets, usually retro-reflective dots or coded markers. In the present study a 3D test object ('Manhattan') has been employed, consisting of a 550x550 mm aluminium baseplate of thickness 10 mm, onto which are affixed 39 anodized aluminium rods of diameter 8 mm and lengths varying from 20 to 305 mm, all perpendicular to the base. Approximately 100 circular retro reflective targets of 2.5 mm diameter are distributed over the baseplate and on the top of each rod. The targets form a rigid array of points in a 3D coordinate space. Under flash illumination the targets are visible in the image from any viewpoint within an incidence angle limit of 50-60 degrees (Fig. 1 right). Eight machine-readable codes are also fixed onto the baseplate to facilitate automatic orientation of the target array in image processing. The targets are conspicuous in the image when the illumination direction is close to the optical axis, which makes a ring light around the lens very effective.

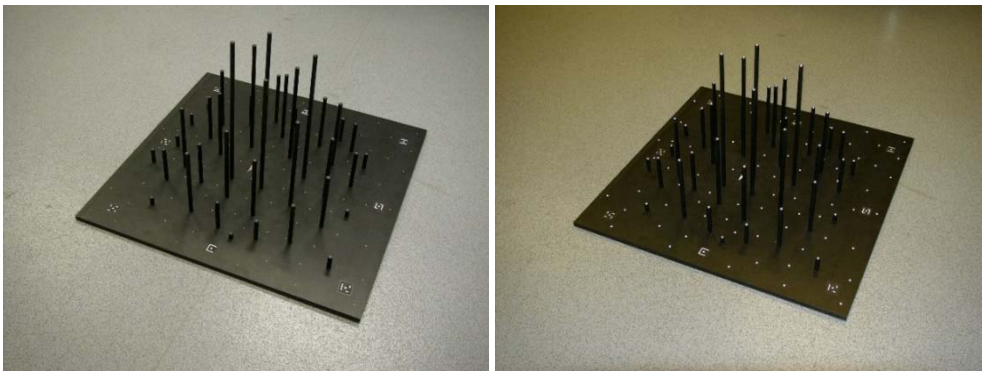

Figure 1: Two views of the 'Manhattan' test object, with targets on vertical rods on an aluminium baseplate: (left) under overhead room lights; (right) illuminated by the inbuilt camera flash, close to the lens.

Starting with initial estimates of camera and target locations and orientation, VMS performs an iterative bundle adjustment to achieve precise results simultaneously for camera calibration parameters, camera locations and orientations, and target coordinates (Granshaw, 1980). The more targets there are, and the more views of the object from independent camera positions, the more accurate the results can be. Shortis *et al* (1995) analysed the best performance that could be expected from a range of target image measurement algorithms including ellipse-fitting, binary centroiding, and Gaussian shape fitting. They concluded that errors of the order of 0.1 pixels were common and that the results would be largely unaffected by quantisation or threshold levels. Any method using grey-scale images was likely to perform an order of magnitude better than with binary (black/white) images.

Figure 2. View of 8-camera test rig in laboratory.

3. Experimental Apparatus

An experimental test rig was constructed in the Advanced Structures Laboratory at UCL (Fig. 2), based on the Newport optical table of surface dimensions 1800(L) x 1200(W) mm. The superstructure consists of four upright solid aluminium pillars with a horizontal canopy of Dexion angle steels, all secured firmly together with 9mm

steel bolts. Diagonal struts of solid 40x8mm bar from the midpoints of the pillars to the canopy sides ensure rigidity of the whole structure. The eight uEye miniature CMOS cameras are mounted at the four corners and four midpoints of the sides of the canopy, hanging down from Manfrotto clamps with swivel heads. The framework outer dimensions are 1500(L) x 1070(W) x 1050(H) mm. The height of each camera above the surface of the optical table is approximately 850 mm.

Each camera is connected by an Ethernet cable to a network gateway, which also provides power. A uEye sync cable enables all cameras to be synchronised by a common trigger signal. The 60mm LED illumination rings are mounted on the front of each camera lens by an adapter ring selected to fit the front diameter (Fig. 3). Power for LEDs is provided by a twin-wire ring supply from a 12-volt 2A transformer, with CCTV plug/socket pairs to enable the cameras to be detached easily. Cable ties retain the bundles of cables in place around the periphery of the canopy.

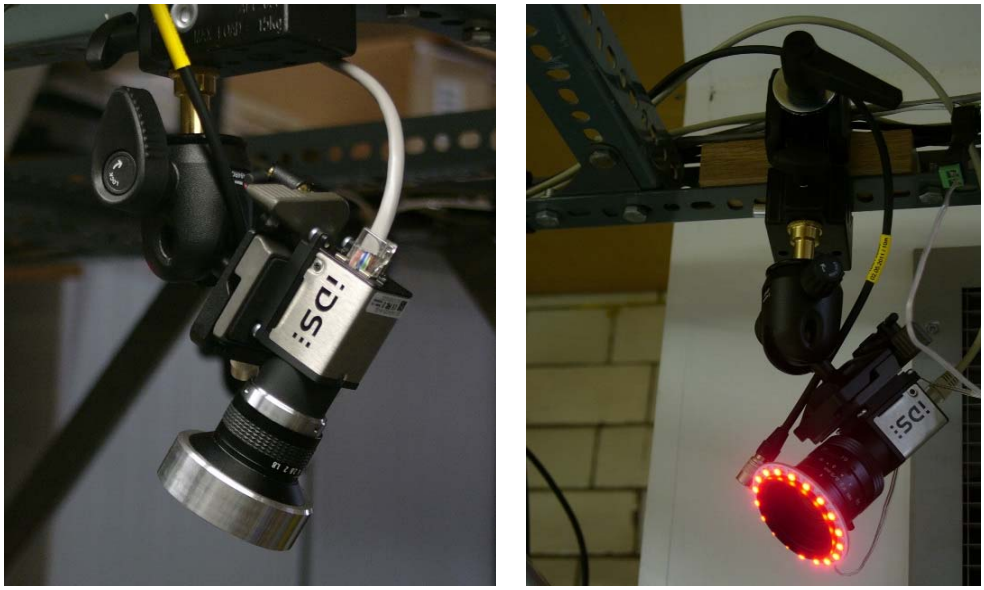

Figure 3. Two views of cameras fitted with C-mount lenses and red LED rings.

The cameras were fitted with six different C-mount lenses of different ages and optical designs, and with focal lengths ranging from 4.8mm to 10mm. The purpose-written software *VMSCapture_uEye* was used to capture the images. The graphic user interface displays live views from all eight cameras, with a slider control for exposure time, as shown in the screen grab in Fig. 4. The images are all upside down because the cameras are mounted upside down, hanging below the canopy.

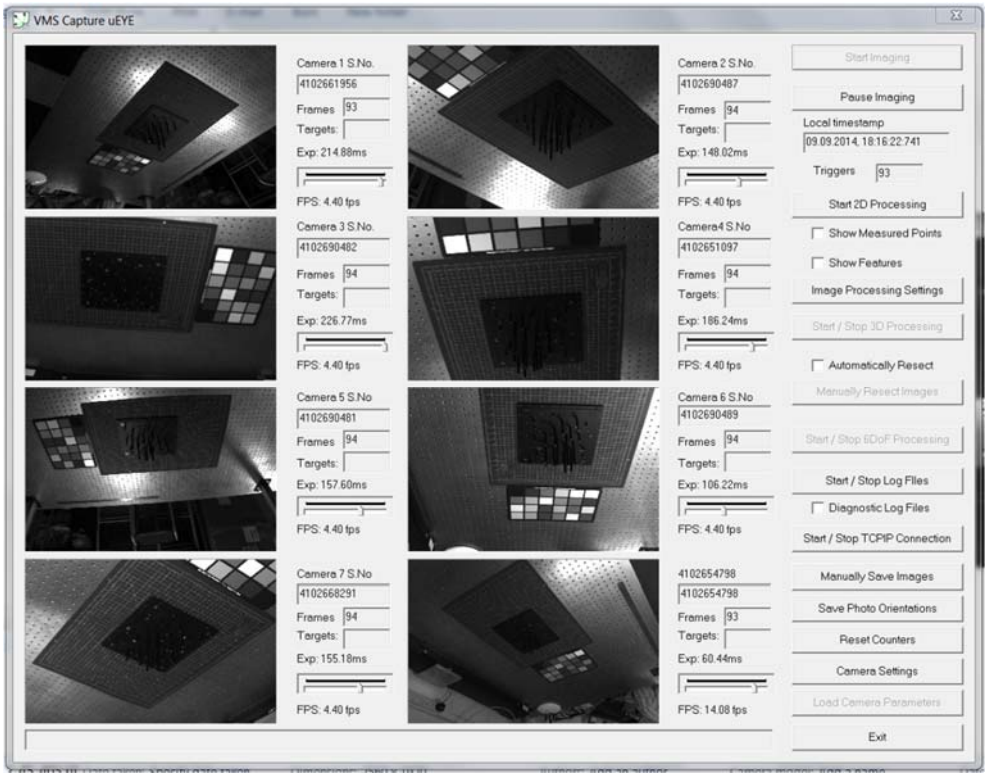

Figure 4. Graphic user interface showing live images from eight cameras.

The software captures eight 12-bit monochrome images simultaneously and saves them as TIFF files (16-bit grey-scale format) of size 2560x1920 pixels. The operation can be either in a 'one-shot' mode, where one image from each camera is captured as a set, or in 'free-run' mode where the image sets are captured continuously at the camera frame rate (typically 3-4 frames/second). When the external trigger signal is applied then all cameras are synchronised and the images are captured simultaneously.

4. Effect of Illumination Wavelength

The Manhattan target object was placed on at the centre of the optical table, within the field of view of all eight cameras. Twelve sets of eight images each were captured, with the test object rotated successively by 90° for four azimuthal angles and tilted at three zenithal angles (0°, 10° and 20° approximately). The images were then analysed by VMS software to determine the camera calibration parameters,

including distortion parameters of each lens. The whole procedure was repeated for LED illumination rings of four different wavelengths: red, green, blue and white. The spectral power distribution of the LEDs was measured with an Ocean Optics USB2000+ spectrometer at intervals of 0.5nm (Fig. 5) and showed that the peak wavelengths of the R,G,B LEDs are at 637, 515 and 442 nm respectively, with bandwidths (FWHM) of 20 nm for both R and B, and 32 nm for G. The white LED has a broad bimodal curve with a small peak at 442 nm (blue) and a broader peak with maximum at 546 nm corresponding to the phosphor emission (yellow-green).

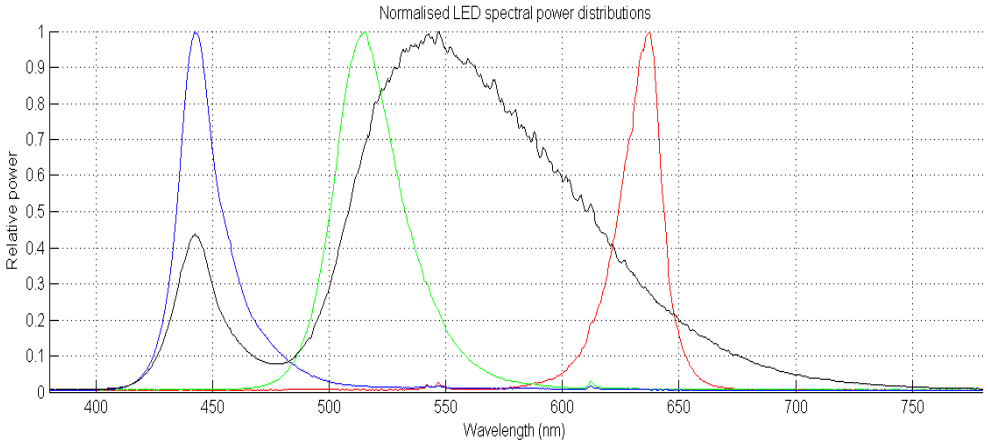

Figure 5. Normalised spectral power distributions of the four LED sources.

In the images analysed by VMS, the mean precision achieved in both image space and object space may be compared for the four LED sources (Table 1). Given that the sensor photosite dimension in the cameras is 2.2 µm, the rms image residual of 0.22 µm represents one tenth of a pixel. Given that the mean distance from all cameras to all targets was 970 mm, the object precision of 4.4 µm (at k=1) represents an overall system discriminating power of approximately 1:220,000. All three narrowband LED sources yielded mean object precisions better than for white light, with an improvement of 10% in the case of red and 5% for green and blue, indicating better optical performance of the lenses.

It should be noted that the network geometries for the four cases were virtually identical, but there were some minor differences leading to the variations observed in image and object space precisions. However all four photogrammetric networks contained very high levels of redundant information, ensuring that the results have commensurately high levels of reliability.

Table 1. RMS image residuals and object space target coordinate precisions at k=1 (µm).

LED source	Red	Green	Blue	White
Image	0.25	0.22	0.22	0.23
Target	4.25	4.45	4.42	4.66

The radial distortion profiles of the lenses, based on the VMS lens distortion models for non-fish-eye and fish-eye lenses (Fig. 6), show that the response for green light was very similar to white, whereas under red light the radial distortion was greater and under blue light it was less. The effect was largely independent of radius, as shown by the ratios of the three lights relative to white (Fig. 6 right). For this lens, a high quality Schneider 8mm, the distortion under red illumination was 5% greater and under blue illumination was 7% less than under green. The ratios differed for the other lenses but the trends were similar. The effect can be explained by lateral chromatic aberration in the optical path, and this is consistent with the results obtained in the previous multispectral study (Robson *et al*, 2014).

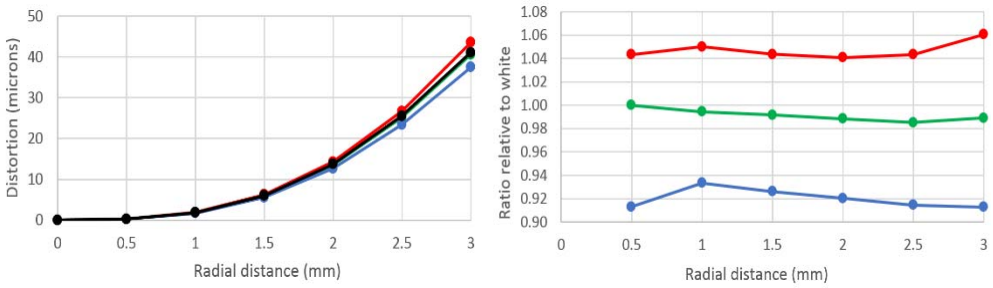

Figure 6. (left) Radial distortion profiles for the Schneider 8mm lens for four LED sources; (right) Ratios of red, green and blue vs white.

Other properties of lenses are also affected by wavelength. Principal distance (PD) in the previous study, using a series of narrow-band transmission filters at 20nm intervals, followed a clear 'parabolic' trend with a minimum at around 500 nm and rising for both shorter and longer wavelengths. This was to be expected for an 'achromat' lens optical design corrected over the range of visible wavelengths to minimise chromatic aberration. In the present study, PD was

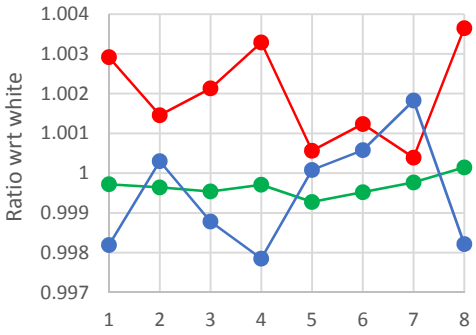

Figure 7. Ratios of principal distance (PD) for red, green and blue vs white LEDs.

calculated as one of the ten parameters of the VMS lens distortion model, for each of the eight lenses under the four LED wavelengths (Table 2). The ratios of the PD values for the red, green and blue sources relative to the white source are plotted in Fig. 7. There is good consistency between the repeated instances of the No-name 5mm lens (numbers 2 and 6) and the Fujinon 9mm lens (numbers 4 and 8). The behaviour for green is stable relative to white, with the ratio close to 1, and in all cases except the fish-eye (Computar 3.8mm, number 7) the PD for blue is less than the PD for red. But it is evident that different lens designs cause them to behave in different ways and a general trend cannot be predicted. The effect of the range of wavelengths is to spread the range of PD by about 0.5% and hence to defocus the image under white light and reduce the precision of the photogrammetric system.

Table 2. Principal distance (PD) for eight lenses under four LED sources.

	Lens	PD (mm)			
1	Schneider 8mm	8.2535	8.2272	8.2146	8.2295
2	No-name 5mm	5.0187	5.0096	5.0129	5.0114
3	Kern 10mm	10.2033	10.1769	10.1692	10.1816
4	Fujinon 9mm	8.9149	8.8831	8.8666	8.8857
5	Schneider 4.8mm	4.9742	4.9678	4.9718	4.9714
6	No-name 5mm	5.0224	5.0138	5.0191	5.0162
7	Computar 3.8mm	3.8363	3.8339	3.8418	3.8348
8	Fujinon 9mm	9.0007	8.9693	8.9520	8.9680

5. Next Steps

The next experimental steps in this research at UCL will be to:

(1) select a model of lens with an acceptable cost/performance trade-off that can be fitted to all cameras to give uniform coverage of the measurement volume;

(2) verify the measurement accuracy of the 8-camera array by using one or more calibrated scale bars in various orientations within the common intersection volume seen by all cameras. For this validation of the system the VDI/VDE 2634 (VDI/VDE 2002) performance specification will be used;

(3) test changes in the performance of the system at a range of temperatures from 15°C to 30°C with precise temperature measurement at an array of points over the metal frame and the air in the light path;

(4) scale up the system by doubling each dimension to a cuboid of approximately 4x2x2 metres and adding a further 8 cameras.

6. Acknowledgement

This investigation was supported by EPSRC grant EP/K018124/1 ‘The Light Controlled Factory’.

7. References

[1] Peggs, G.N., Maropoulos, P.G., Hughes, E.B., Forbes, A.B., Robson, S., Ziebart, M. and Muralikrishnan, B. (2009). Recent developments in large-scale dimensional metrology. *Proc. Inst. Mechanical Engineers, Part B: Journal of Engineering Manufacture*, 223(6):571-595.

[2] Mallon, J. and Whelan, P.F. (2007) Calibration and removal of lateral chromatic aberration in images. *Pattern Recognition Letters*, pp. 125-135.

[3] Luhmann, T., Hastedt, H., Tecklenburg, W. (2006) Modelling of Chromatic Aberration for High Precision Photogrammetry. *ISPRS Archives*, Vol. XXXVI, Part 5:173-178.

[4] Robson, S., MacDonald, L.W., Kyle, S. and Shortis, M. (2014) Multispectral calibration to enhance the metrology performance of C-mount camera systems. *Proc. ISPRS Conf. on Close-range Imaging, Ranging and Applications*, Riva del Garda: 517-521.

[5] Luhmann, T., (2011) 3D imaging: how to achieve highest accuracy. *Proc. Conf. on Videometrics, Range Imaging, and Applications XI*, SPIE Vol. 8085-02.

[6] Shortis, M.R., Ogleby, C.L., Robson, S., Karalis, E.M. and Beyer H.A. (2001) Calibration modelling and stability testing for the Kodak DC200 series digital still camera, *Proc. SPIE Conf. on Videometrics and Optical Methods for 3D Shape Measurement*, Vol. 4309:148-153.

[7] Granshaw, S.E. (1980) Bundle adjustment methods in engineering photogrammetry, *Photogrammetric Record* 10(56):181-207.

[8] Shortis, M.R., Clarke, T.A. and Robson, S. (1995) Practical testing of the precision and accuracy of target image centering algorithms, *Proc. SPIE Conf. on Videometrics IV*, Vol. 2598, 65.

[9] VDI/VDE (2002) VDI/VDE 2634 Part 1 *Optical 3D Measuring Systems – Imaging Systems with Point-by-point Probing.* Beuth Verlag, Berlin.